© 2014. Published by The Company of Biologists Ltd | Journal of Cell Science (2014) 127, 1007–1017 doi:10.1242/jcs.137273

RESEARCH ARTICLE

Myosin Vb and Rab11a regulate phosphorylation of ezrin in enterocytes

Herschel S. Dhekne[1,‡], Nai-Hua Hsiao[1,‡], Pieter Roelofs[1], Meena Kumari[1], Christiaan L. Slim[1], Edmond H. H. M. Rings[2,*] and Sven C. D. van IJzendoorn[1,§]

ABSTRACT

Microvilli at the apical surface of enterocytes allow the efficient absorption of nutrients in the intestine. Ezrin activation by its phosphorylation at T567 is important for microvilli development, but how such ezrin phosphorylation is controlled is not well understood. We demonstrate that a subset of kinases that phosphorylate ezrin closely co-distributes with apical recycling endosome marker Rab11a in the subapical domain. Expression of dominant-negative Rab11a mutant or depletion of the Rab11a-binding motor protein myosin Vb prevents the subapical enrichment of Rab11a and these kinases and inhibits ezrin phosphorylation and microvilli development, without affecting the polarized distribution of ezrin itself. We observe a similar loss of the subapical enrichment of Rab11a and the kinases and reduced phosphorylation of ezrin in microvillus inclusion disease, which is associated with *MYO5B* mutations, intestinal microvilli atrophy and malabsorption. Thus, part of the machinery for ezrin activation depends on recycling endosomes controlled by myosin Vb and Rab11a which, we propose, might act as subapical signaling platforms that enterocytes use to regulate development of microvilli and maintain human intestinal function.

KEY WORDS: Apical, Enterocyte, Microvilli, Microvillus inclusion disease, Recycling endosome

INTRODUCTION

The establishment of apical–basal cell surface asymmetry, or cell polarity, is a crucial step in the development and maintenance of functional epithelial tissues. In parallel with the establishment of the apical plasma membrane domain, organelles also adopt a polarized distribution in epithelial cells. Well-known is the Golgi complex, which in polarized epithelial cells is typically positioned between the nucleus and the apical plasma membrane domain. In addition, a subpopulation of the recycling endosomal system, characterized by the presence of the small guanosine triphosphatase (GTPase) Rab11a, is enriched in close proximity to the apical surface (Goldenring et al., 1996). Recent work has demonstrated that these Rab11a-positive recycling endosomes play an important role in the biogenesis of the apical plasma membrane domain and, in particular, ensure its specific macromolecular composition (Apodaca et al., 2012; Bryant et al., 2010; Gálvez-Santisteban et al., 2012; Golachowska et al., 2010; Winter et al., 2012).

In addition to its specific protein and lipid composition, numerous densely and uniformly packed finger-like projections filled with actin filament bundles that are tethered to the subapical actin web, called microvilli, represent a prominent structural feature of the apical plasma membrane. Microvilli are highly dynamic and can grow and shrink. Proteins move up and down the microvilli membrane in response to signals and microvilli generate vesicles that are shed into the apical lumen (McConnell et al., 2009) where they regulate epithelial–microbial interactions (Shifrin et al., 2012). Interestingly, (part of) the molecular pathway(s) for the development of microvilli has been demonstrated to constitute a separate branch of the epithelial cell polarity program driven by the serine/threonine liver kinase B1 (LKB1) (Gloerich et al., 2012; ten Klooster et al., 2009). Whether the apically enriched Rab11a-positive recycling endosomes play a direct role in the development and organization of microvilli at the apical plasma membrane is not known.

Members of the ezrin–radixin–moesin (ERM) protein family and some of their interaction partners play a key role in the organization of the apical plasma membrane and microvilli development in various types of epithelial cells (Fehon et al., 2010; LaLonde et al., 2010; Wang et al., 2006). Of these, ezrin is a protein-threonine kinase substrate and the only ERM protein expressed in the enterocytes of the small intestine (Berryman et al., 1993; Saotome et al., 2004). Loss of ezrin expression in the embryonic and adult mouse intestine causes microvillus atrophy and villus fusions (Casaletto et al., 2011; Saotome et al., 2004). Ezrin is present in a closed (inactive) and an open (active) conformation. In its active conformation, the N-terminal domain of ezrin binds integral proteins of the apical plasma membrane and peripheral proteins at the cytosolic side of the apical surface, whereas its C-terminal domain binds actin filaments (Bretscher et al., 1997). The conversion from an inactive to an active conformation and the exclusive apical localization of ezrin requires phosphorylation of T567 (Bretscher et al., 1997; Fehon et al., 2010; Matsui et al., 1998). Microvilli abundance and/or length correlate well with the extent of ezrin phosphorylation. Several kinases have been implicated in the direct T567 phosphorylation of ezrin in intestinal epithelial cells, including protein kinase B2/Akt2 (Shiue et al., 2005), atypical protein kinase C-iota (aPKCι) (Wald et al., 2008), mammalian Sterile 20 (Ste20)-like kinase-4 (Mst4) (Gloerich et al., 2012; ten Klooster et al., 2009), lymphocyte-oriented kinase (LOK) and Ste20-like kinase (SLK) (Viswanatha et al., 2012). Knockdown of each of

[1]Department of Cell Biology, University of Groningen, University Medical Center Groningen, Groningen, The Netherlands. [2]Department of Pediatrics, University of Groningen, University Medical Center Groningen, Groningen, The Netherlands.
*Present address: Erasmus Medical Center Rotterdam, Erasmus University Rotterdam, Rotterdam, The Netherlands.
‡These authors contributed equally to this work.

§Author for correspondence (s.c.d.van.ijzendoorn@umcg.nl)

Received 21 June 2013; Accepted 9 December 2013

Journal of Cell Science

Journal of Cell Science (2014) 127, 1007–1017 doi:10.1242/jcs.137273

these kinases in various intestinal epithelial cell models inhibits microvillus development at the apical plasma membrane (Gloerich et al., 2012; Shiue et al., 2005; ten Klooster et al., 2009; Viswanatha et al., 2012; Wald et al., 2008). Some of these kinases have been reported to localize to the apical microvillus membrane (Shiue et al., 2005; Viswanatha et al., 2012). By contrast, other ezrin-phosphorylating kinases appear to, at least partially, localize to undefined intracellular compartments. For instance, following the activation of the polarity protein LKB1, Mst4 phosphorylates T567 in ezrin after being translocated to the enterocyte subapical domain by an unknown mechanism (ten Klooster et al., 2009). Also, the location of the active aPKCι is not clear while its activating kinase phosphoinositide-dependent kinase-1 (PDK1) associates with apical endosomes (Mashukova et al., 2012).

Here, we investigated the contribution of the apical endosomal system to ezrin activation and the development of microvilli in intestinal epithelial cells. We demonstrate that (1) aPKCι and Mst4 closely co-distribute with Rab11a and are enriched beneath the apical surface; (2) that Rab11a activity and the Rab11a effector and actin-based motor protein myosin Vb maintain this subapical position of Rab11a-positive recycling endosomes; and (3) that loss of myosin Vb function in intestinal epithelial cell lines, as well as in patients carrying *MYO5B* mutations, causes an aberrant localization of Rab11a-positive recycling endosomes with a concomitant inhibition of ezrin phosphorylation and microvilli development.

RESULTS

The ezrin-phosphorylating kinases Mst4 and aPKCι co-distribute with Rab11a in the subapical domain of intestinal epithelial cells

Phosphorylation of ezrin at T567 is a crucial step in its activation that is required for development and organization of apical microvilli. The kinases Akt2, LOK and SLK, which have been implicated in phosphorylation of ezrin, localize to the apical plasma membrane domain (Shiue et al., 2005; Viswanatha et al., 2012). For other kinases, the localization is less clear. We examined the subcellular distribution of two kinases, the Ste20 family kinase Mst4 of the germinal center kinase III (GCKIII) family of kinases, and atypical aPKCι, which have been demonstrated to function in ezrin phosphorylation and microvilli development at the apical plasma membrane of intestinal epithelial LS174T-W4 and Caco-2 cells, respectively (Gloerich et al., 2012; ten Klooster et al., 2009; Wald et al., 2008). In villus intestinal epithelial cells in human duodenal biopsies, endogenous Mst4 localized just below the apical actin-rich microfilament zone at the apical aspect of the enterocytes. Line plots confirmed that the fluorescence intensity of Mst4 (green line) peaked subjacent to the (filamentous actin labeled) apical surface (Fig. 1A, red line), indicating that Mst4 localized to intracellular compartments. Double-labeling experiments demonstrated that a significant fraction of Mst4 closely co-distributed with Rab11a in the apical cytoplasm (Fig. 1B, Mst4 labeling pseudo-colored magenta in panel 3; white color in panel 5 indicates colocalization; Mander's coefficient 0.82). Equally, a significant fraction of Rab11a co-distributed with Mst4 (Mander's coefficient 0.74). Fluorescence intensity plots of enlarged regions shown in Fig. 1B5 demonstrate that Mst4 and Rab11a closely co-distribute in discrete structures (Fig. 1C,D). Quantification analysis of the double labeling was carried out by intensity correlation analysis (ICA). ICA addresses the staining relationship between two probes, which is represented as the product of the differences from the mean (PDM) for each pixel (Li et al., 2004) (Fig. 1B6). PDM values are positive when the intensity of two fluorescent probes vary together in an image (dependently), whereas negative PDM values reflect pixel intensities that vary asynchronously. The visibly subcellular co-appearance of Mst4 and Rab11a in conjunction with the quantitative analyses (Fig. 1B–D) demonstrated that significant fractions of the kinases and Rab11a co-distributed at the light microscopic level in discrete structures in the subapical domain of the enterocytes. Double-labeling and intensity-correlation analyses showed less colocalization of Mst4 with Rab8, another marker of recycling endosomes that was more scattered throughout the cytoplasm (supplementary material Fig. S1). Similar to Mst4, endogenous T555-phosphorylated (activated) aPKCι was also enriched at the apical domain of human enterocytes, whereas total endogenous aPKCι was distributed more throughout the cytoplasm (supplementary material Fig. S2). As seen in line plots, the fluorescence intensity of (T555-phosphorylated) aPKCι (Fig. 1E, red line) peaked subjacent to the (F-actin-labeled; Fig. 1E, green line) apical surface, where it partly colocalized with the recycling endosome marker Rab11a (Fig. 1F–H; white color in panel F5 and PDM images in panel F6 indicate colocalization). These data demonstrate that significant pools of Mst4 and T555-phosphorylated aPKCι co-distribute with subapically enriched Rab11a in intestinal epithelial cells.

The enrichment of Mst4 and Rab11a in the subapical domain is required for ezrin-T567 phosphorylation

Given that two kinases previously implicated in ezrin phosphorylation and microvillus development at the apical surface of enterocytes (Gloerich et al., 2012; ten Klooster et al., 2009; Wald et al., 2008) closely co-distributed with the apical recycling endosome marker Rab11a, we hypothesized that the subcellular position of these endosomes in close proximity to the apical plasma membrane (cf. Fig. 1) could contribute to ezrin phosphorylation and microvilli development at the apical surface. In order to test this hypothesis, we used intestinal epithelial LS174T-W4 cells in which doxycycline-induced expression of the pseudo-kinase STRAD and resultant activation of the polarity protein LKB1 stimulates the overnight development of single-cell apical–basolateral polarity (Baas et al., 2004; Gloerich et al., 2012; ten Klooster et al., 2009). It is well established in these cells that Mst4 is important for ezrin phosphorylation and that the LKB1-triggered translocation of Mst4 to the subapical domain correlates with ezrin phosphorylation and microvillus formation (Gloerich et al., 2012; ten Klooster et al., 2009). However, the intracellular compartments and machinery responsible for this translocation are unknown. In non-induced (non-polarized) LS174T-W4 cells, Mst4 and aPKCι (supplementary material Fig. S3, red) as well as Rab11a (supplementary material Fig. S3, green) appeared randomly distributed throughout the cytoplasm, and co-distribution of the kinases and Rab11a supported by PDM images was observed (supplementary material Fig. S3, −dox, yellow arrows indicate positive PDM puncta). aPKCι was also found in the nucleus, which has been reported previously in other cell types (Sabherwal et al., 2009). Some T567-phosphorylated ezrin was randomly localized to the cell cortex (supplementary material Fig. S3, −dox, top row). By contrast, following doxycycline-induced Stradα expression and LKB1 activation (ten Klooster et al., 2009) aPKCι and Mst4 (Fig. 2A, red) translocated together with Rab11a (Fig. 2A, green) to sharply defined areas just beneath the cell cortex (Fig. 2A, +dox, arrows).

Journal of Cell Science (2014) 127, 1007–1017 doi:10.1242/jcs.137273

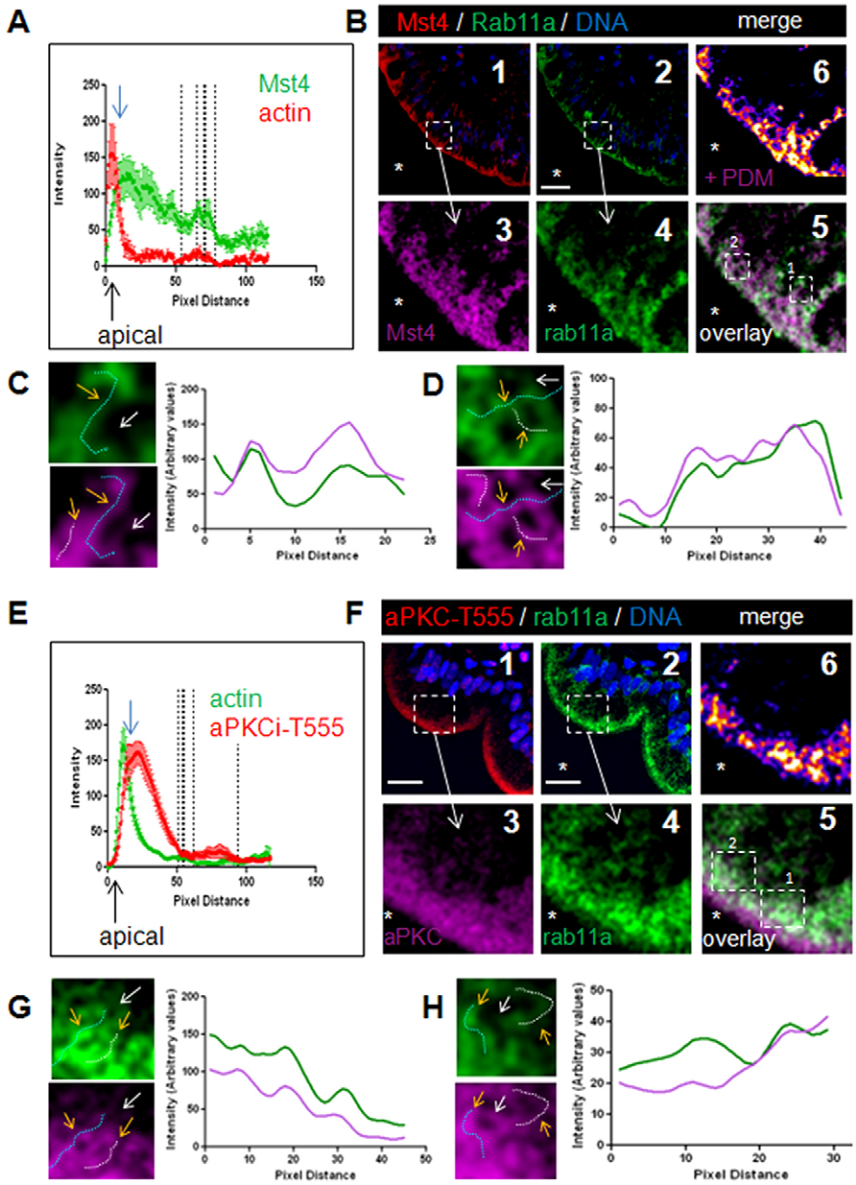

Fig. 1. Subcellular distribution of Mst4 and aPKCι in *in vivo* enterocytes. (A) Line plots showing the relative distribution of Mst4 versus actin along the apical–basal axis of *in vivo* enterocytes. (B) Double labeling for Mst4 (1,3; in 3, Mst4 is pseudo-colored magenta) and Rab11a (2,4). Overlay image is shown in panel 5, where white color indicates colocalization. Positive (+) PDM image representing quantitative analysis of colocalization is shown in panel 6. (C,D) Enlargements of the boxes indicated in B, panel 5 and indicated fluorescence intensity plots of Mst4 and Rab11a. (E) Line plots showing the relative distribution of aPKCι versus actin along the apical–basal axis of *in vivo* enterocytes. (F) Double labeling for aPKCι (1,3; in 3, aPKCι is pseudo-colored magenta) and Rab11a (2,4). Overlay image is shown in panel 5, where white color indicates colocalization. Positive (+) PDM image is shown in panel 6. (G,H) Enlargements of the boxes indicated in F, panel 5 and indicated fluorescence intensity plots of aPKCι and Rab11a. Asterisks indicate the position of the intestinal lumen. Scale bars: 10 μm.

PDM images supported the polarized co-distribution of Rab11a and the kinases (Fig. 2A). Notably, at those site(s) beneath the cell cortex where aPKCι, Mst4 and Rab11a co-accumulated, increased phosphorylation of ezrin at T567 (Fig. 2A, red) and development of microvilli was apparent (Fig. 2A, +dox, arrows).

To further investigate the apparent relationship between the subapical enrichment of Rab11a and Mst4 on the one hand and ezrin phosphorylation at the apical domain on the other hand, we disrupted the microtubule network in doxycycline-induced (polarized) cells with nocodazole. Microtubule disruption has previously been demonstrated to disperse Rab11a-positive endosomes in polarized Madin–Darby canine kidney (MDCK) cells (Casanova et al., 1999). Nocodazole effectively disrupted the microtubule organization in LS174T-W4 cells, as evidenced by a change from a filamentous to punctate β-tubulin staining pattern (supplementary material Fig. S4A). Nocodazole did not inhibit the percentage of cells that displayed a clearly defined ezrin- (Fig. 2B; top row) or actin-enriched (Fig. 2C) surface cap. By contrast, nocodazole caused the dispersion of Rab11a (Fig. 2B, bottom row) and Mst4 (Fig. 2C, bottom row) and abolished their enrichment at the subapical domain. Concomitantly, nocodazole-treated cells displayed a significant reduction in the fluorescence intensity of phosphorylated ezrin labeling (Fig. 2D). The fluorescence intensity of phosphorylated ezrin was reduced, with ∼50% in nocodazole-treated cells, and the percentage of nocodazole-treated cells that displayed a distinguishable T567-phosphorylated ezrin cap was reduced by ∼30% when compared with non-treated control cells (supplementary material Fig. S4B).

We then treated doxycycline-induced LS174T-W4 cells with brefeldin A, an inhibitor of ADP-ribosylating factors (Arfs), which have previously been shown to control the organization of Rab11a-positive endosomes (Kondo et al., 2012; Shin et al., 2004). In brefeldin-A-treated cells, Mst4 was no longer enriched at the apical surface domain, but accumulated with Rab11a in distinct punctate structures (Fig. 2E, yellow arrows). Although a fraction of Rab11a maintained its subapical enrichment, without the co-enrichment of Mst4 in brefeldin-A-treated cells (Fig. 2E, white arrow), this did not coincide with local stimulation of ezrin phosphorylation (Fig. 2E, white arrow, and supplementary

Journal of Cell Science (2014) 127, 1007–1017 doi:10.1242/jcs.137273

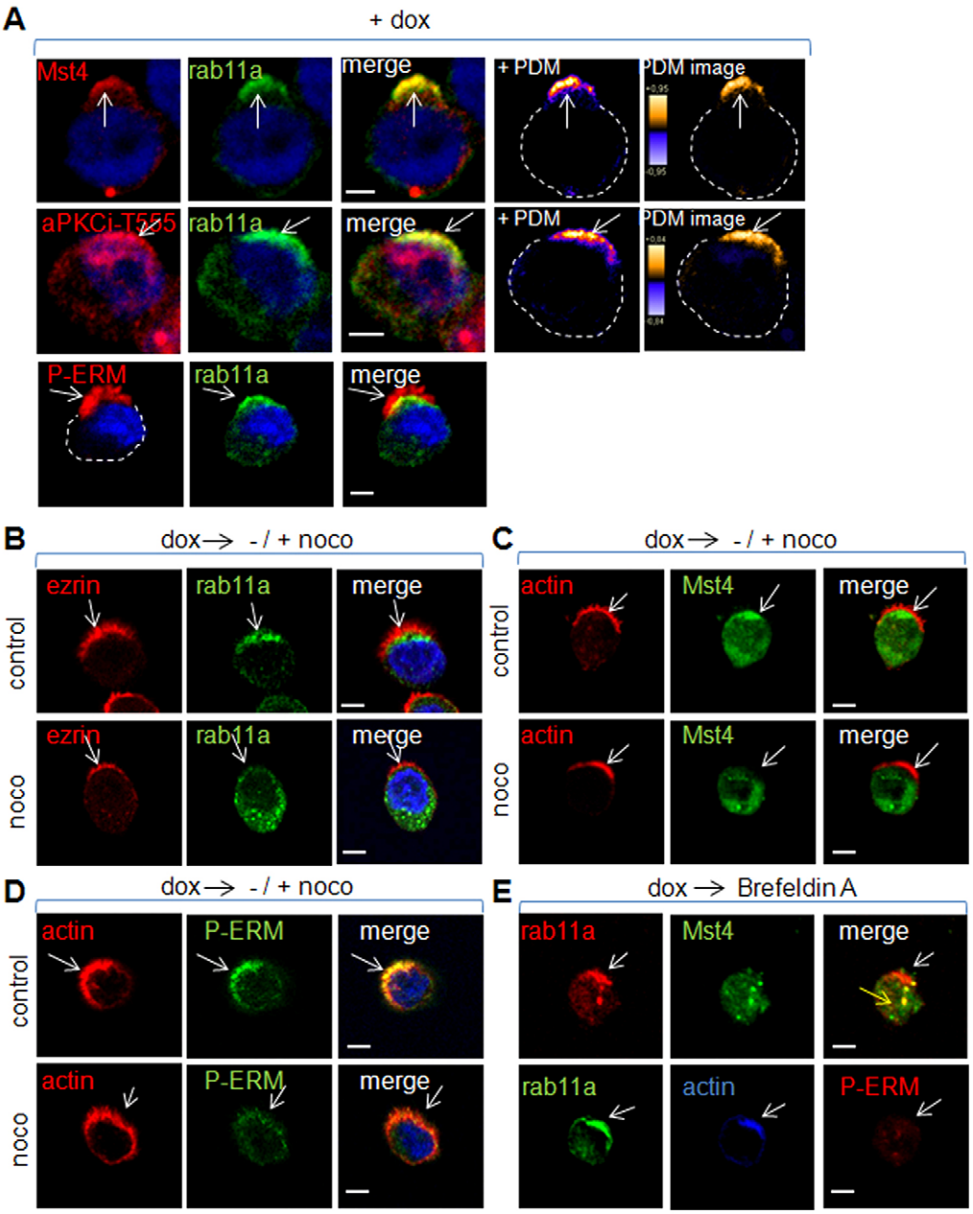

Fig. 2. Local cortical enrichment of Rab11a and ezrin kinases correlates with local ezrin phosphorylation. (A) Co-distribution of Mst4, aPKCι and T567-phospho-ERM (all in red) with Rab11a (green) in induced (+dox) LS174T-W4 cells (arrows indicate co-distribution). Mst4, Rab11a, merged and positive (+) PDM images are presented. Dashed lines mark the outline of the cells. (B) Nocodazole (noco; 33 μM at 37˚C for 1 hour) disperses Rab11 endosomes (in green) without inhibiting the polarized distribution of ezrin (in red) in doxycycline-induced cells when compared with non-treated control doxycycline-induced cells (arrows indicate apical domain). (C) Nocodazole (noco) disperses Mst4 (in green) without inhibiting the polarized distribution of cortical actin filaments (in red) in doxycycline-induced cells when compared with non-treated control doxycycline-induced cells (arrows indicate apical domains). (D) Nocodazole (noco) inhibits local ezrin phosphorylation (in green) in doxycycline-induced cells when compared with non-treated control doxycycline-induced cells (arrows indicate apical domain). (E) Brefeldin A (BFA; 100 ng/ml at 37˚C for 1 hour) causes accumulation of Mst4 with Rab11a in intracellular puncta whereas part of the Rab11a maintains its local cortical accumulation (top row). Brefeldin A (BFA) inhibits local ezrin phosphorylation at the cortical site where Rab11a accumulates (bottom row). Scale bars: 5 μm.

material Fig. S4C). These data indicate that it is the subapical enrichment of Mst4 together with Rab11a rather than that of Rab11a as such that is required to stimulate local cortical ezrin phosphorylation.

Taken together, these data demonstrate an intimate relationship between (1) the translocation to and accumulation of Rab11a, Mst4 and aPKCι at defined regions of the cell cortex and (2) ezrin T567 phosphorylation at those regions.

Rab11a and myosin Vb control the subapical enrichment of Mst4 and ezrin phosphorylation at the apical surface

The molecular mechanisms responsible for the apical enrichment of Rab11a-positive recycling endosomes in polarized epithelial cells are not well understood (Winter et al., 2012), but probably involve the interaction of Rab11a-positive recycling endosomes with the cytoskeleton. Rab11a at recycling endosomes, when in its GTP-bound state, interacts with its effector and actin-filament-based motor protein myosin Vb (Lapierre et al., 2001) which, in non-polarized cells has been reported to function as a tether for peripheral endocytic compartments (Kapitein et al., 2013; Provance et al., 2008). In order to determine whether myosin Vb was involved in the subapical enrichment of Rab11a-positive recycling endosomes and, hence, that of Mst4 and aPKCι in intestinal epithelial cells, we inhibited the expression of myosin Vb by RNA interference (supplementary material Fig. S5). Infection of cells with short hairpin (sh)RNA against myosin Vb in LS174T-W4 cells [visualized by expression of green fluorescent protein (GFP); see Methods] did not reduce the percentage of cells that displayed a polarized ezrin-enriched cap (Fig. 3A,G). The inhibition of myosin Vb expression, however, effectively prevented the doxycycline-triggered polarized translocation of Rab11a (Fig. 3B,C, red; supplementary material Fig. S8), aPKCι (Fig. 3B, green; supplementary material Fig. S8), Mst4 (Fig. 3C, green; supplementary material Fig. S8) and PDK1 (supplementary material Figs S6 and S8) to the cell cortex, whereas non-infected GFP-negative cells were unaffected (supplementary material Figs S6–S8; compare with Fig. 2A, +dox). Moreover, knockdown of myosin Vb inhibited the local

Journal of Cell Science (2014) 127, 1007–1017 doi:10.1242/jcs.137273

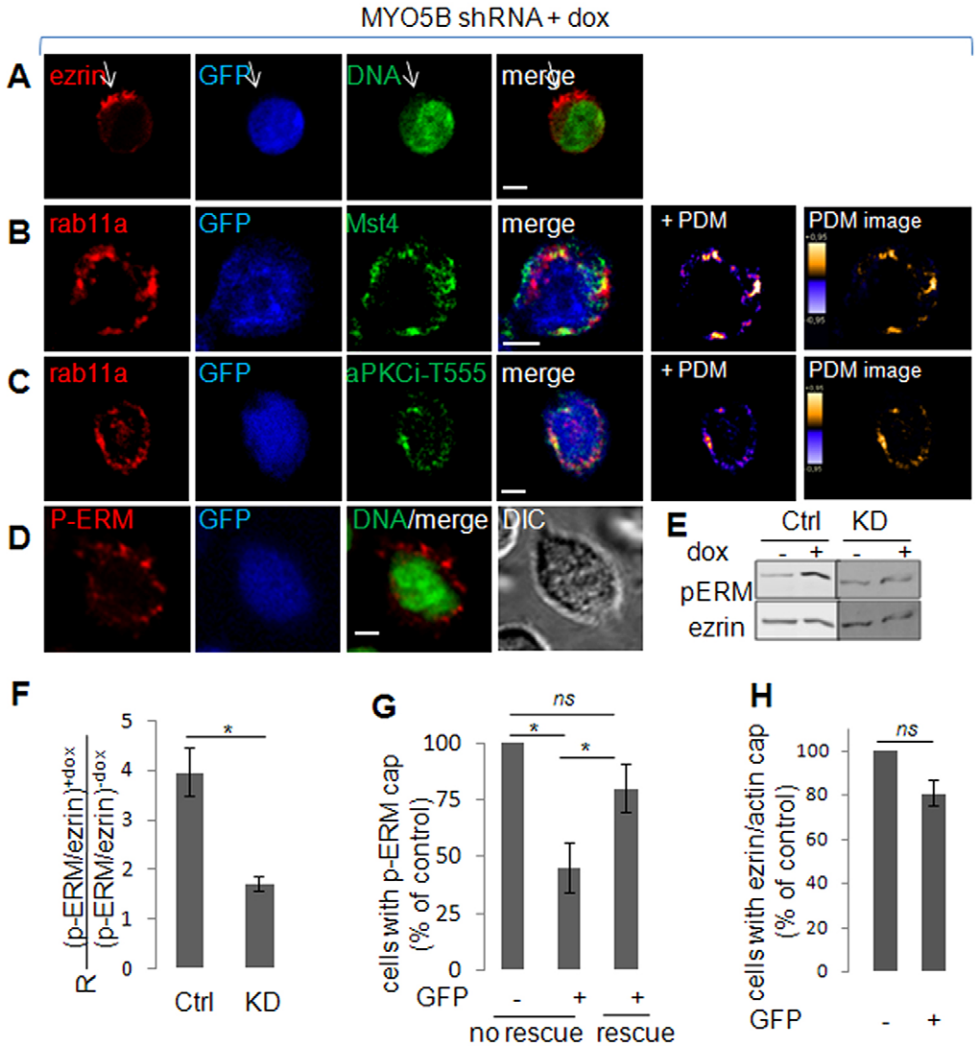

Fig. 3. Myosin Vb knockdown prevents the subapical enrichment of endosomes and kinases and inhibits local ezrin phosphorylation. (A) Infection of LS174T-W4 cells with shRNA against myosin Vb (GFP-positive cells) does not prevent the polarized distribution of ezrin at the plasma membrane. (B,C) Infection of LS174T-W4 cells with shRNA against myosin-Vb (GFP-positive cells) prevents the polarized translocation of T555-aPKCι (B) and Mst4 (C) with Rab11a endosomes to the plasma membrane. (D) Infection of LS174T-W4 cells with shRNA against myosin Vb (GFP-positive cells) inhibits local cortical ezrin phosphorylation. Compare with uninfected (GFP-negative) cells or cells infected with shRNA against luciferase (supplementary material Fig. S3). Arrows indicate the apical surface domain. (E) pERM and ezrin expression in doxycycline-induced control and myosin-Vb-knockdown LS174T-W4 cells. (F) Calculated ratio (p-ERM/total ezrin) in doxycycline-induced cells/ (pERM/total ezrin) in non-induced cells. (G) Percentage of LS174T-W4 cells that show doxycycline-stimulated ezrin phosphorylation at the cortex. (H) Percentage of cells that show an ezrin or actin-positive apical cap. *$P<0.05$; *ns*, not significant. KD, knockdown. Scale bars: 5 μm.

stimulation of T567 phosphorylation of ezrin at the plasma membrane as evidenced by immunofluorescence microscopy and western blot analyses (Fig. 3D–H), and this effect was completely rescued by the reintroduction of shRNA-resistant full-length human myosin Vb (Fig. 3F). In support of these data, a dominant-negative GDP-locked mutant of EGFP-Rab11a that cannot bind myosin Vb failed to translocate to the cell cortex and inhibited ezrin phosphorylation (Fig. 4A, top row) without inhibiting the polarized distribution of ezrin (Fig. 4A, top row; Fig. 4B–E). As a control, we transfected cells with wild-type EGFP–Rab11a (Fig. 4B–E) or a constitutively active EGFP–Rab11a mutant (Fig. 4A, bottom row; Fig. 4B–E), which did not display inhibitory effects on the translocation and subapical enrichment of EGFP-Rab11a and ezrin phosphorylation. Similar to our observations in single LS174T-W4 cells, infection of monolayers of intestinal epithelial Caco-2 cells with lentivirus producing shRNA against myosin Vb (supplementary material Fig. S4) resulted in a significant reduction of T567-phosphorylated ezrin at the apical domain when compared with control Caco-2 cells (Fig. 5B,C), as evidenced by immunofluorescence microscopy and western blot analyses. We did not observe these effects following the infection of cells with lentivirus producing shRNA against luciferase as a negative control (Fig. 5A,C). Knockdown of myosin Vb in Caco-2 cells resulted in generally more sparse and disorganized apical microvilli and an increase in the apical cell surface area that displayed virtually no microvilli, as evidenced by scanning electron microscopy (Fig. 5D–F). The monolayer organization of the cells was maintained under these conditions as shown by the unchanged distribution of the tight-junction-associated zona occludens (ZO)-1 protein at the apex of the cell lateral surfaces (supplementary material Fig. S9). Collectively, these data demonstrate that myosin Vb and Rab11a control the subapical enrichment of Mst4 and aPKCι and, concomitantly, contribute to the extent of T567 phosphorylation in ezrin at the apical plasma membrane and brush border development in cultured intestinal epithelial cell lines. Furthermore, our data indicate that this process is uncoupled from the establishment and maintenance of a local enrichment of ezrin.

Redistribution of Rab11a-positive recycling endosomes and inhibition of ezrin phosphorylation in enterocytes of patients with Microvillus inclusion disease

Mutations in the gene encoding myosin Vb (*MYO5B*) have been identified in patients with microvillus inclusion disease (MVID) (Erickson et al., 2008; Müller et al., 2008; Szperl et al., 2011), a

Journal of Cell Science (2014) 127, 1007–1017 doi:10.1242/jcs.137273

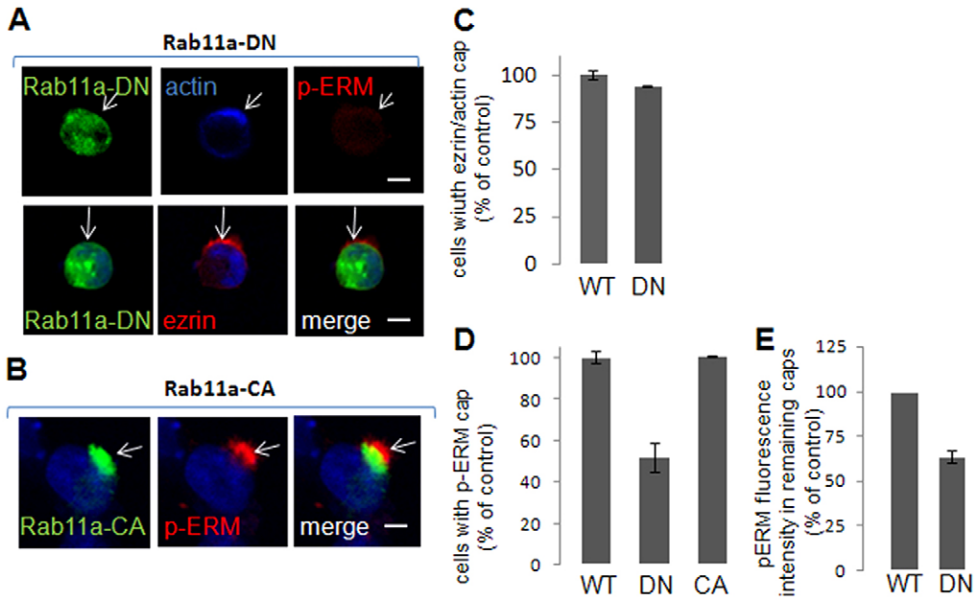

Fig. 4. Effects of Rab11a mutants on Rab11a distribution and ezrin phosphorylation. (A) Dominant-negative EGFP–Rab11a (Rab11a-DN; green) fails to accumulate at the actin (blue)- or ezrin (red)-enriched apical domain (white arrows) and inhibits local cortical ezrin phosphorylation (red). (B) Constitutively active EGFP–Rab11a (Rab11a-CA) has no inhibitory effect. Arrows indicate apical surface domain. (C) Quantification of the percentage of cells expressing EGFP–Rab11a-WT, DN, or CA that show an ezrin- or actin-positive cap, or (D) show a p-ERM-positive apical cap. (E) pERM fluorescence intensity in the remaining pERM caps. Scale bars 5 μm.

rare and fatal disease characterized by intestinal malabsorption and microvillus atrophy (Cutz et al., 1989; Phillips and Schmitz, 1992; Ruemmele et al., 2006). However, neither the T567 phosphorylation status of ezrin nor the distribution of Mst4 and aPKCι has been examined in MVID enterocytes. This was investigated in tissue from a previously reported MVID patient carrying a homozygous *MYO5B* nonsense mutation (c.4366C>T, p.1456X) that results in reduced mRNA expression, and the resultant protein is predicted to lack Rab11a-binding sites (Szperl et al., 2011). In contrast to the subapical localization of Mst4 in age-matched control human enterocytes (cf. Fig. 1A), Mst4 was not observed at the subapical domain of MVID enterocytes but, instead, was redistributed with Rab11a to the supranuclear region (Fig. 6A,B). The apical cytoplasm of MVID enterocytes was largely devoid of Rab11a, supporting the data from cultured cells that myosin Vb controls the translocation of Rab11a-positive recycling endosomes to the apical plasma membrane domain (cf. Fig. 3B). In MVID enterocytes, Mst4 and Rab11a both redistributed to the supranuclear region (Fig. 6A,B) where they showed considerable overlap (Fig. 6B–D). Mst4 colocalized at a few puncta with transferrin receptor (TfR) (supplementary material Fig. S10A) and some colocalization of Mst4 with Rab8 (supplementary material Fig. S10B) and with the cis-Golgi matrix protein GM130 (supplementary material Fig. S10C) was

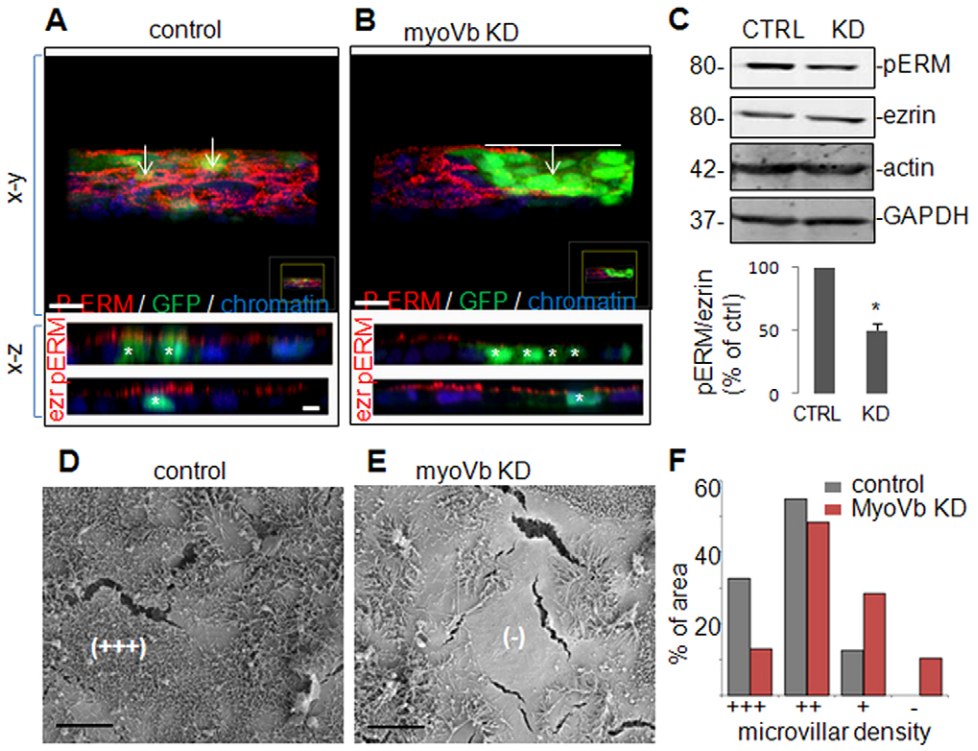

Fig. 5. Effect of myosin Vb shRNA on ezrin phosphorylation and microvilli organization in Caco-2 cells. (A,B) Immunofluorescence labeling of T567-phosphorylated ERM (large tilted *x-y* and top *x-z* image) and ezrin (bottom *x-z* image) in control (D) and myosin-Vb-knockdown (E) cells. GFP (green) labels transduced cells. Arrows and asterisks in *x-y* and *x-z* images, respectively, show the presence (A) or absence (B) of T567-phosphorylated ERM. (C) Expression of ezrin, T567-phosphorylated ezrin, actin and GAPDH. (D,E) Representative scanning electron micrographs of the apical surface of control and myosin-Vb-knockdown cells. (F) Semi-quantitative analysis of microvilli density per unit surface area, on a scale from '+++' (very dense; see D for a representative +++ surface area) to '−' (no microvilli; see E for a representative − surface area). Scale bars: 10 μm.

Journal of Cell Science (2014) 127, 1007–1017 doi:10.1242/jcs.137273

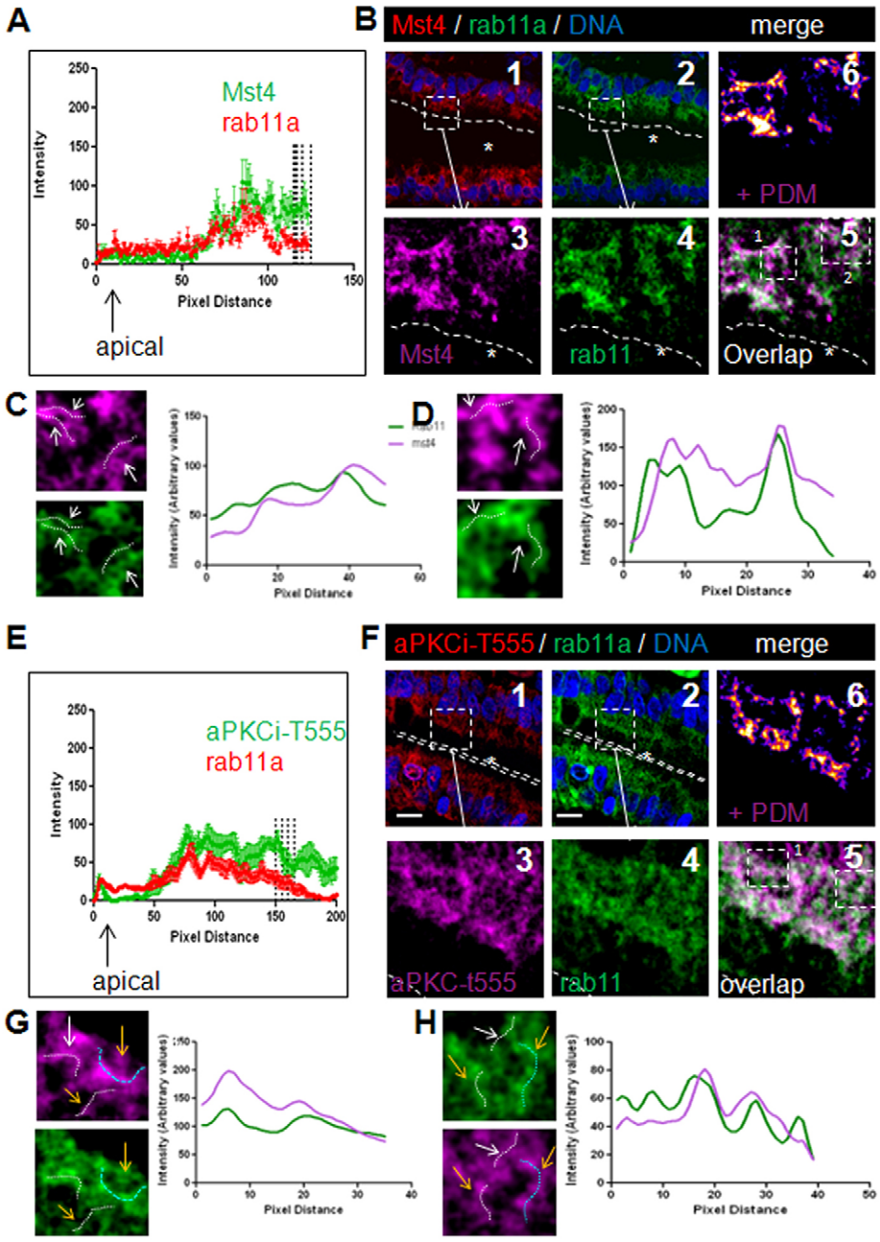

Fig. 6. Subcellular distribution of Mst4 and aPKCι in *in vivo* MVID enterocytes. (A) Line plots showing the relative distribution of Mst4 versus actin along the apical-basal axis of *in vivo* MVID enterocytes. (B) Double labeling for Mst4 (1,3; in 3, Mst4 is pseudo-colored magenta) and Rab11a (2,4). Overlay image is shown in B5 where white color indicates colocalization. Positive (+) PDM image representing quantitative analysis of colocalization is shown in panel 6. (C,D) Enlargements of the boxes indicated in B, panel 5 and indicated fluorescence intensity plots of Mst4 and Rab11a. (E) Line plots showing the relative distribution of aPKCι versus actin along the apical–basal axis of *in vivo* enterocytes. (F) Double labeling for aPKCι (1,3; in 3, aPKCι is pseudo-colored magenta) and Rab11a (2,4). Overlay image is shown in panel 5, where white color indicates colocalization. Positive (+)PDM is shown in panel 6. (G,H) Enlargements of the boxes indicated in F, panel 5 and indicated fluorescence intensity plots of aPKCι and Rab11a. Arrows indicate areas of colocalization; asterisks indicate the position of the intestinal lumen. Scale bars: 10 μm.

observed; the latter is consistent with the previously reported interaction between both proteins. Similar to Mst4, we did not observe T555-phosphorylated aPKCι at the apical domain of MVID enterocytes (cf. Fig. 1E–H) but, instead, aPKCι-T555 and Rab11a redistributed together to the supranuclear region (Fig. 6E–H). Total aPKCι remained uniformly and diffusely distributed across the MVID enterocytes and overall fluorescence intensity of T555-phosphorylated aPKCι did not change (supplementary material Fig. S11A,B), suggesting that the phosphorylation of aPKCι at T555 in recycling endosomes had occurred in a different location. Consistent with this, PDK1, the kinase responsible for phosphorylating aPKCι at T555 (Mashukova et al., 2012), displayed a similar supranuclear re-localization with Rab11a in MVID enterocytes (supplementary material Fig. S11C).

When examining the phosphorylation status and localization of ezrin in MVID enterocytes, we detected only minimal T567-phosphorylated ezrin in most of the MVID enterocytes, in contrast to the predominant expression of T567-phosphorylated ezrin at the apical surface of control enterocytes (Fig. 7A). Although phosphorylated ezrin at the apical plasma membrane of MVID enterocytes was noticeably absent (Fig. 7A), some enterocytes showed phosphorylated ezrin in the sub-apical cytoplasm that colocalized with actin and therefore might represent microvillus inclusions (Fig. 7A, top insert). In addition to a reduction in T567-phosphorylated ezrin, ezrin itself was mislocalized from a predominant apical surface localization to intracellular compartments (Fig. 7B). Furthermore, apical actin was disorganized (Fig. 5A, insert) and a reduction in the colocalization of ezrin and actin was observed. In agreement with these data, we observed severe microvillus atrophy by transmission electron microscopy analysis of duodenal biopsies (Fig. 7C). Finally, we observed in the MVID duodenum (not earlier recognized) fusions of villi (Fig. 7D, black arrows) and

Journal of Cell Science (2014) 127, 1007–1017 doi:10.1242/jcs.137273

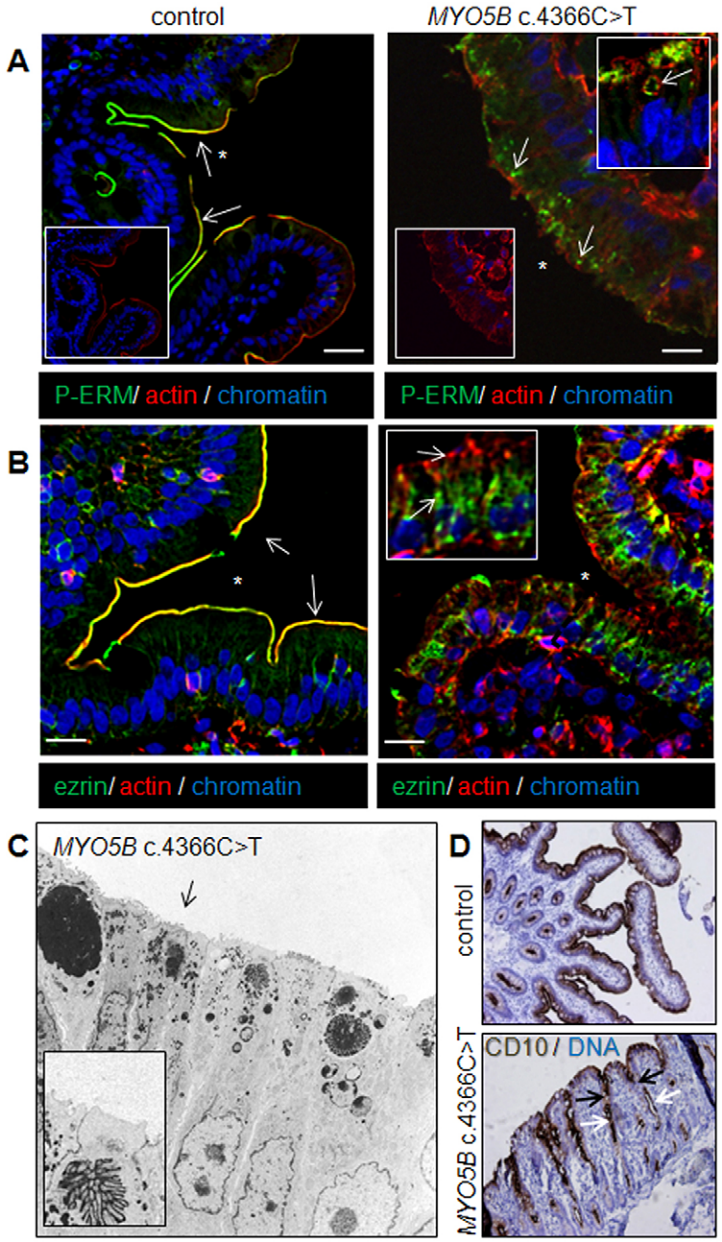

Fig. 7. Ezrin phenotypes in the MVID intestine. (A) T567-phosphorylated ERM, actin and DNA in control and MVID enterocytes. (B) Ezrin, actin and DNA in control and MVID enterocytes. Bottom inserts in A, actin/chromatin staining alone. Top insert in right micrograph in A, actin and T567-phosphorylated ERM-decorated microvillus inclusion (arrow) observed in another part of the same specimen. Insert in B is an enlargement of an area highlighting the absence of colocalization of the two proteins (arrows). Arrows in B, A (left panel) show areas of colocalization. Arrows in A (right panel) show subapically localized T567-phosphorylated ERM. Asterisks indicate the lumen. (C) Representative electron micrograph of MVID enterocytes. Insert shows an enlargement of the microvillus inclusion. Arrows indicate the apical surface. (D) CD10 and hematoxylin staining in control and MVID intestine. Black and white arrows indicate villi fusions and secondary apical lumens, respectively. Scale bars: 10 μm.

formation of secondary apical lumens (Fig. 7D, white arrows), which are prominent features of the intestine in ezrin-knockout mice (Casaletto et al., 2011; Saotome et al., 2004). Together with the results from cultured cells, these data indicate that *MYO5B* mutations in the enterocytes of MVID patients cause the redistribution of Rab11a-positive recycling endosomes and ezrin-phosphorylating kinases away from the apical plasma membrane domain and, concomitantly, inhibit the T567-phosphorylation of ezrin, brush border formation and possibly villus architecture.

DISCUSSION

The structural and compositional identity of the apical plasma membrane of intestinal epithelial cells is crucial for the exchange of molecules with the gut lumen and essential for survival. As the predominant structural apical surface specializations, microvilli play an important role in intestinal epithelial function, and loss of apical microvilli correlates with several intestinal diseases involving malabsorption and cancer. Many *in vitro* and *in vivo* studies have implicated the actin-organizing scaffold protein ezrin, its interacting proteins, and subapical actin filament organization as a pivotal component of the machinery controlling microvilli development and organization at the apical surface of epithelial cells (reviewed by Fehon et al., 2010). The activation of ezrin by phosphorylation at T567, which allows the protein to unfold and link actin filaments to the apical surface, is a prerequisite for proper microvilli development. Various kinases can phosphorylate ezrin and stimulate microvilli development in intestinal epithelial cells and, evidently, these kinases need to be in close proximity to ezrin. Some of these kinases, such as LOK, SLK and Akt2, have been demonstrated to localize in the microvilli membrane at the apical surface (Shiue et al., 2005; Viswanatha et al., 2012), whereas the localization of other kinases, notably aPKCι and Mst4, was not clear. Here, we demonstrated that aPKCι-T555 (as well as its activating kinase PDK1) and Mst4, previously demonstrated to contribute to apical T567 phosphorylation and localization of ezrin and consequently

Journal of Cell Science (2014) 127, 1007–1017 doi:10.1242/jcs.137273

to apical microvilli formation in intestinal epithelial cells (Wald et al., 2008; ten Klooster et al., 2009; Gloerich et al., 2012), did not localize predominantly to the apical surface. Instead, these kinases co-distributed both *in vivo* and *in vitro* with Rab11a, a small GTPase that predominantly decorates apical recycling endosomes, in discrete compartments beneath the apical plasma membrane domain.

We reasoned that if the subapical enrichment of these Rab11a-positive endosomes and the kinases contributed to the T567 phosphorylation of ezrin, then the misplacement of these endosomes would be predicted to inhibit ezrin phosphorylation and microvilli development at the apical domain. The molecular mechanisms that control the position of Rab11a-positive recycling endosomes in intestinal epithelial cells are not well understood (Winter et al., 2012). Here, we demonstrated with shRNA-mediated knockdown and subsequent rescue experiments that loss of the actin-based motor and Rab11a effector protein myosin Vb effectively prevents the subapical enrichment of Rab11a-positive recycling endosomes, as well as that of Mst4 and aPKCι, in intestinal epithelial cells without inhibiting the LKB1-induced cell polarization process. In agreement with these results, the expression of a dominant negative Rab11a mutant that is unable to bind myosin Vb prevented the polarized positioning of Rab11a-positive endosomes in these cells at the apical domain without perturbing the polarized enrichment of ezrin. Of interest, we did not observe a focused clustering of Rab11a around the centrosome after loss of myosin Vb function, as previously shown for ciliated cells (Lapierre et al., 2001; Roland et al., 2011), which suggests a different organization of the apical cytoplasm and cytoskeleton in the (non-ciliated) enterocytes. The loss of Rab11a-positive endosomes from the apical domain of the cells following knockdown of myosin Vb might reflect a defective tethering of the endosomes at the cell periphery (Kapitein et al., 2013; Provance et al., 2008) or a defect in the collective surface-directed movement of the recycling endosomal system, as has been proposed recently for the collective outward movement of Rab11 recycling endosomes in oocytes (Schuh, 2011). In line with recent reports (Gloerich et al., 2012; ten Klooster et al., 2009), the inhibition of Mst4 positioning following the overexpression of dominant-negative Rab11a or knockdown of myosin Vb resulted in the inhibition of ezrin T567 phosphorylation and microvilli formation. It should be noted that this inhibition of ezrin phosphorylation was not complete, which could be due to the presence of additional ezrin T567-phosphorylating kinases such as LOK, SLK and/or Akt2 (Shiue et al., 2005; Viswanatha et al., 2012). Multiple kinases possibly act (together or in a spatiotemporal regulated manner) to control the extent of ezrin T567 phosphorylation, which directly relates to the density and uniformity of microvilli at brush border surfaces (Zhu et al., 2008). Our data suggest that Rab11a and myosin Vb control the apical enrichment of Mst4 and aPKCι and, in this way, contribute to the T567 phosphorylation of ezrin at the apical plasma membrane domain and brush border development. It should be noted that although quantitative image analyses clearly demonstrated that significant fractions of the kinases and Rab11a colocalize in polarized enterocytes at the light microscopic level, immunoelectron microscopy will be needed to unambiguously determine whether the kinases directly associate with the membrane of Rab11a-decorated apical recycling endosomes or whether they are dependent on Rab11a/myosin Vb in a different way for their subapical enrichment. Nonetheless, the observation that experimental manipulation of the subcellular redistribution of Rab11a (with myosin Vb shRNA, Rab11a mutants, nocodazole) was closely matched by a similar redistribution of the kinases indicates their dependent localization. This process is uncoupled from the establishment and maintenance of apical surface polarity as such. It is of interest to note that loss of Rab11a or myosin Vb function in hepatocytes did inhibit cell polarity (Wakabayashi et al., 2005), which raises intriguing questions about the role of the apical recycling endosomal system in relation to aspects of apical polarity in different types of epithelial cells (Golachowska et al., 2012).

An important finding was that Rab11a was similarly depleted from the apical cytoplasm and accumulated in the supranuclear region of enterocytes of a patient diagnosed with MVID and carrying a homozygous mutation in the *MYO5B* gene (Szperl et al., 2011). In addition, Mst4 and aPKCι were displaced with Rab11a from the apical domain to the supranuclear region. These observations in MVID enterocytes are consistent with a defective subcellular positioning of Rab11a-positive recycling endosomes and of the kinases to the apical domain of the cells, in agreement with our myosin-Vb-knockdown experiments. Concomitant with the supranuclear retention of the kinases, the T567 phosphorylation and predominant apical localization of ezrin, the only ERM protein family member in the small intestine (Berryman et al., 1993; Saotome et al., 2004), was inhibited in MVID enterocytes. These findings in MVID enterocytes underscore the (patho)physiological relevance of brush border control by recycling endosomes.

Knockout of ezrin in the mouse intestine not only affected microvilli but also caused villus fusions (Casaletto et al., 2011; Saotome et al., 2004). Analysis of small intestinal biopsies of two MVID patients revealed villi fusions at discrete spots along their lateral domain. Secondary lumens – apical lumens that appeared not exposed to the gut lumen – accompanied the villus fusions in the MVID intestine. The combined villus and microvillus defects probably cause a severe reduction in the absorptive capacity of the intestine in MVID. The comparable defects in villus architecture in the intestine of ezrin-knockout mice (Casaletto et al., 2011; Saotome et al., 2004) and MVID (this study) further support the idea that ezrin loss of function as a downstream consequence of myosin Vb loss of function is part of MVID pathogenesis. Notably, phenotypic differences also exist between the small intestine in ezrin-knockout mice and MVID patients. Brush border enzymes, such as alkaline phosphatase and sucrase isomaltase, accumulated intracellularly in MVID enterocytes (Cutz et al., 1989; Phillips et al., 1985; Phillips et al., 2004), but remained at the apical surface of intestinal epithelial cells in ezrin-knockout mice (Casaletto et al., 2011; Saotome et al., 2004). Furthermore, microvillus inclusions have not been reported in the enterocytes of ezrin-knockout mice (Saotome et al., 2004). Loss of apical ezrin phosphorylation might thus account for the microvillus atrophy but not for the intracellular retention of brush border proteins and microvillus inclusions in MVID enterocytes. In line with the demonstration that brush border development in intestinal epithelial cells constitutes a separate branch of the apical–basal polarity program (Gloerich et al., 2012; ten Klooster et al., 2009), these phenotypic hallmarks of MVID might therefore be uncoupled at the mechanistic level downstream of loss of myosin Vb function.

Recently, a novel function for recycling endosomes, in addition to their classical role in vesicular trafficking, as multifunctional platforms on which molecular machines are assembled to suit different cellular functions was proposed (Gould and Lippincott-Schwartz, 2009). In line with this, our collective data support a

model in which Rab11a, through its interaction with myosin Vb, maintains a subapical signaling platform in the form of apical recycling endosomes that allows Mst4 and aPKCι to contribute to the activation of ezrin and, in this way, contribute to the (dynamic) structural organization of the intestinal brush border membrane (see model in supplementary material Fig. S12).

METHODS

Cell culture

LS417T-W4 and Caco-2 cell culture was as described previously (Gloerich et al., 2012; ten Klooster et al., 2009).

Immunofluorescence labelling of tissues and cells

Cells were fixed with 3.7% paraformaldehyde at room temperature for 20 minutes. Cells were incubated with 0.1 M glycine in PBS for 20 minutes, permeabilized with 0.2% Triton X-100 for 10 minutes and blocked with 3% FCS in PBS for 1 hour and incubated with primary antibodies at 37℃ for 2 hours, except for anti-Rab11a antibodies (4℃ for 16 hours). Cells were incubated with Cy5- or Alexa-Fluor-543-conjugated secondary antibodies and DRAQ5/DAPI at 37℃ for 30 minutes. Sections of formalin-fixed samples were deparaffinised, rehydrated, washed with PBS and subjected to epitope retrieval with citric acid pH 6.0 in a microwave for 20 minutes. Non-specific binding sites were blocked with 5% FCS in PBS overnight. Primary antibodies (supplementary material Table S1) were diluted in blocking solution with 0.05% Tween-20 at 37℃ for 2 hours followed by incubation with Alexa-Fluor-488- or Alexa-Fluor-543-conjugated secondary antibodies. Nuclei were stained with DRAQ5. All slides were mounted with DAKO mounting medium.

Fluorescence microscopy and analysis

Specimens were examined and images were taken with a TCS SP2 AOBS CLSM (Leica). Image analysis and histogram adjustments were performed with MacBiophotonics ImageJ. For tissue staining, images were processed by Huygens Pro deconvolution software using classical maximum likelihood estimation (CMLE) with a theoretical PSF calculated by feeding the microscope settings. The channel backgrounds or channel were set at 30 and quality change threshold at 0.3%, which reduced background without losing resolution. To isolate brighter features, output images were processed using Gaussian Filter plug-in (value 0.7) in MBP ImageJ. For quantification of colocalization, the JACOP plug-in for ImageJ was used. In brief, shot noise for each channel was arithmetically subtracted from raw images. Non-specific staining was arithmetically subtracted. Images were median filtered (value 1.5), and individual cells were analysed for colocalization using Mander's correlation coefficient with threshold set as described earlier (Pollock et al., 2010). As a negative control, the Mander's coefficient was determined for colocalization of the protein of interest with the nuclear stain DRAQ5. As a positive control (set to 100% colocalization), the Mander's coefficient was determined by using one primary antibody and two secondary antibodies tagged with Alexa Fluor 488 and Alexa Fluor 543 against the primary antibody. Student's *t*-test was used to determine statistical significance between conditions. PDM images were obtained by processing raw images for shot noise, background subtraction by median filter, thresholding (as mentioned above) and using Intensity correlation analysis (ICA) plug-in (with crosshair of 3 pixels). Pseudo-colouring was done by changing LUTs to magenta and green. Segmented line ROIs were drawn on linear structures on one channel and profile plots were made for corresponding channels. The line plots for indicating LS174t-W4 cells and tissue were made by connecting dots of means with s.e.m. error bars in Graphpad prism. Fluorescent intensities of pERM in apical brush borders were quantified by defining ROIs around the caps in the corresponding actin channels and mean fluorescent intensity quantified.

Electron microscopy

Freshly obtained biopsy samples were processed for transmission electron microscopy as described (Szperl et al., 2011). For scanning electron microscopy, cells were fixed with 2% glutaraldehyde in 0.1 M sodium cacodylate overnight at 4℃ and post-fixed with 1% osmium tetroxide in 0.1 M cacodylate buffer at room temperature for 1 hour. After dehydration, samples were critical-point dried from carbon dioxide and sputter-coated with 5 nm palladium/gold, and imaged at 2 kV using a JEOL-JSM6301F scanning electron microscope.

Myosin Vb knockdown and rescue experiments

The shRNA target sequence, region 2333–2351 of human *MYO5B* cDNA (target sequence GGCTGCAGAAGGTGAAATA) was cloned into the shRNA expression vector. A target sequence in the luciferase gene was used as a control. For rescue experiments, full-length human *MYO5B* was cloned, after which the shRNA target sequence was mutated (5′-ggctTcaAaa AgtTaaata-3′, mutations in capitals) by site-directed mutagenesis (QuikChange, Agilent Technologies). ShRNA-resistant *MYO5B* cDNA was introduced into the lentiviral expression vector pLenti-CMV/TO-Hygro-DEST, by recombination. DNA sequencing was performed at each step of cloning (ServiceXS, The Netherlands). PCR reactions were performed according to manufacturer's instructions for Vent DNA polymerase (NEB). The cloned *MYO5B* gene does not contain ExonD.

For the production of lentivirus, HEK293T cells were plated onto poly-L-Lysine-coated plates in DMEM supplemented with 10% FCS and 1% sodium pyruvate. Cells were transfected with CMVdR8.1, VSV-G and pMID-i-2 using CaCl2 and Hank's balanced salt solution. Medium was changed after 17 hours. After 24 hours, virus-containing medium was collected, filtered and stored at −80℃. Caco-2 cells were transduced with lentivirus diluted in DMEM with 10% FCS. Expression of GFP in cells was indicative of successful transduction, as also evidenced by reduced myosin Vb mRNA. In other experiments, Caco-2 cells were plated on Transwell filters (Corning, 0.4 µm pore size) and 48 hours later, transduced with virus in the presence of polybrene for 16 hours, and cultured for another 4 days. LS417T-W4 cells were transduced with lentivirus for knockdown (supplementary material Fig. S1A) on two consecutive days and after 48 hours were trypsinized and plated in the presence (or absence) of doxycycline for 16 hours.

Cell transfection

LS174T-W4 cells were transfected with EGFP-Rab11a-WT, EGFP-Rab11a-DN or EGFP-Rab11a-CA mutants (a gift from Dr R. E. Pagano, Mayo Clinic and Foundation, Rochester, MN) (Choudhury et al., 2002) using Lipofectamine2000 (Invitrogen) following the manufacturer's protocols.

qRT-PCR

RNA was extracted from cells following the manufacturer's instructions (Invisorb Spin Cell RNA mini kit, Westburg). cDNA was synthesized using poly-dT primer and SuperscriptII reverse transcriptase (Invitrogen) following the manufacturer's protocol. qRT primers were designed by using Primer-3 (http://frodo.wi.mit.edu) (supplementary material Table S1). Reactions were run on an ABI7500 (Applied Biosystems). Cycling conditions comprised 15 minutes of polymerase activation at 95℃ and 40 cycles at 95℃ for 15 seconds and 60℃ for 30 seconds.

Western blot analysis

Cells were lysed using ice-cold lysis buffer (RIPA, 150 mM sodium chloride, 1% Triton X-100, 0.5% sodium deoxycholate, 0.1% SDS, 50 mM Tris-HCl, pH 8.0) with protease inhibitors (Sigma). Protein concentration was determined (Bio-Rad). For western blotting of phospho-ERM or phospho-aPKCι, cells were lysed by directly adding 100 µl of 2× SDS-Laemmli buffer on ice for 10 minutes, after which the lysate was boiled for 5 minutes, centrifuged at 13,000 rpm and stored at −80℃. 30–50 µg protein was separated on a 7.5% acrylamide gel and blotted onto nitrocellulose membrane. Blots were blocked with 3% BSA blocking solution for 1 hour, incubated with primary appropriate secondary antibodies, and analyzed on an Odyssey Li-Cor infra-red scanner.

Acknowledgements

We thank the patients, their parents, and the transplantation teams of the University Medical Center Groningen. We thank J. Kuipers for expert technical assistance with scanning electron microscopy, Dr R.E. Pagano for Rab11a constructs, and Dr H. Clevers and Dr J.L. Bos for the LS517T-W4 cells and protocols.

Competing interests
The authors declare no competing interests.

Author contributions
H.D., N.H., P.R., M.K. and C.S. performed the experiments. H.D., E.R. and S.v.I.J. designed the experiments and wrote the manuscript.

Funding
This study was supported by the Dutch Digestive Disease Foundation (Maag Lever Darm Stichting, MLDS) [grant number WO 08-17 to E.R.].

Supplementary material
Supplementary material available online at
http://jcs.biologists.org/lookup/suppl/doi:10.1242/jcs.137273/-/DC1

References
Apodaca, G., Gallo, L. I. and Bryant, D. M. (2012). Role of membrane traffic in the generation of epithelial cell asymmetry. *Nat. Cell Biol.* **14**, 1235-1243.
Baas, A. F., Kuipers, J., van der Wel, N. N., Batlle, E., Koerten, H. K., Peters, P. J. and Clevers, H. C. (2004). Complete polarization of single intestinal epithelial cells upon activation of LKB1 by STRAD. *Cell* **116**, 457-466.
Berryman, M., Franck, Z. and Bretscher, A. (1993). Ezrin is concentrated in the apical microvilli of a wide variety of epithelial cells whereas moesin is found primarily in endothelial cells. *J. Cell Sci.* **105**, 1025-1043.
Bretscher, A., Reczek, D. and Berryman, M. (1997). Ezrin: a protein requiring conformational activation to link microfilaments to the plasma membrane in the assembly of cell surface structures. *J. Cell Sci.* **110**, 3011-3018.
Bryant, D. M., Datta, A., Rodríguez-Fraticelli, A. E., Peränen, J., Martín-Belmonte, F. and Mostov, K. E. (2010). A molecular network for de novo generation of the apical surface and lumen. *Nat. Cell Biol.* **12**, 1035-1045.
Casaletto, J. B., Saotome, I., Curto, M. and McClatchey, A. I. (2011). Ezrin-mediated apical integrity is required for intestinal homeostasis. *Proc. Natl. Acad. Sci. USA* **108**, 11924-11929.
Casanova, J. E., Wang, X., Kumar, R., Bhartur, S. G., Navarre, J., Woodrum, J. E., Altschuler, Y., Ray, G. S. and Goldenring, J. R. (1999). Association of Rab25 and Rab11a with the apical recycling system of polarized Madin-Darby canine kidney cells. *Mol. Biol. Cell* **10**, 47-61.
Choudhury, A., Dominguez, M., Puri, V., Sharma, D. K., Narita, K., Wheatley, C. L., Marks, D. L. and Pagano, R. E. (2002). Rab proteins mediate Golgi transport of caveola-internalized glycosphingolipids and correct lipid trafficking in Niemann-Pick C cells. *J. Clin. Invest.* **109**, 1541-1550.
Cutz, E., Rhoads, J. M., Drumm, B., Sherman, P. M., Durie, P. R. and Forstner, G. G. (1989). Microvillus inclusion disease: an inherited defect of brush-border assembly and differentiation. *N. Engl. J. Med.* **320**, 646-651.
Erickson, R. P., Larson-Thomé, K., Valenzuela, R. K., Whitaker, S. E. and Shub, M. D. (2008). Navajo microvillous inclusion disease is due to a mutation in MYO5B. *Am. J. Med. Genet. A.* **146A**, 3117-3119.
Fehon, R. G., McClatchey, A. I. and Bretscher, A. (2010). Organizing the cell cortex: the role of ERM proteins. *Nat. Rev. Mol. Cell Biol.* **11**, 276-287.
Gálvez-Santisteban, M., Rodriguez-Fraticelli, A. E., Bryant, D. M., Vergarajauregui, S., Yasuda, T., Bañón-Rodríguez, I., Bernascone, I., Datta, A., Spivak, N., Young, K. et al. (2012). Synaptotagmin-like proteins control the formation of a single apical membrane domain in epithelial cells. *Nat. Cell Biol.* **14**, 838-849.
Gloerich, M., ten Klooster, J. P., Vliem, M. J., Koorman, T., Zwartkruis, F. J., Clevers, H. and Bos, J. L. (2012). Rap2A links intestinal cell polarity to brush border formation. *Nat. Cell Biol.* **14**, 793-801.
Golachowska, M. R., Hoekstra, D. and van IJzendoorn, S. C. D. (2010). Recycling endosomes in apical plasma membrane domain formation and epithelial cell polarity. *Trends Cell Biol.* **20**, 618-626.
Golachowska, M. R., van Dael, C. M. L., Keuning, H., Karrenbeld, A., Hoekstra, D., Gijsbers, C. F. M., Benninga, M. A., Rings, E. H. H. M. and van Ijzendoorn, S. C. D. (2012). MYO5B mutations in patients with microvillus inclusion disease presenting with transient renal Fanconi syndrome. *J. Pediatr. Gastroenterol. Nutr.* **54**, 491-498.
Goldenring, J. R., Smith, J., Vaughan, H. D., Cameron, P., Hawkins, W. and Navarre, J. (1996). Rab11 is an apically located small GTP-binding protein in epithelial tissues. *Am. J. Physiol.* **270**, G515-G525.
Gould, G. W. and Lippincott-Schwartz, J. (2009). New roles for endosomes: from vesicular carriers to multi-purpose platforms. *Nat. Rev. Mol. Cell Biol.* **10**, 287-292.
Kapitein, L. C., van Bergeijk, P., Lipka, J., Keijzer, N., Wulf, P. S., Katrukha, E. A., Akhmanova, A. and Hoogenraad, C. C. (2013). Myosin-V opposes microtubule-based cargo transport and drives directional motility on cortical actin. *Curr. Biol.* **23**, 828-834.
Kondo, Y., Hanai, A., Nakai, W., Katoh, Y., Nakayama, K. and Shin, H.-W. (2012). ARF1 and ARF3 are required for the integrity of recycling endosomes and the recycling pathway. *Cell Struct. Funct.* **37**, 141-154.
LaLonde, D. P., Garbett, D. and Bretscher, A. (2010). A regulated complex of the scaffolding proteins PDZK1 and EBP50 with ezrin contribute to microvillar organization. *Mol. Biol. Cell* **21**, 1519-1529.
Lapierre, L. A., Kumar, R., Hales, C. M., Navarre, J., Bhartur, S. G., Burnette, J. O., Provance, D. W., Jr, Mercer, J. A., Bähler, M. and Goldenring, J. R. (2001). Myosin vb is associated with plasma membrane recycling systems. *Mol. Biol. Cell* **12**, 1843-1857.
Li, Q., Lau, A., Morris, T. J., Guo, L., Fordyce, C. B. and Stanley, E. F. (2004). A syntaxin 1, Galpha(o), and N-type calcium channel complex at a presynaptic nerve terminal: analysis by quantitative immunocolocalization. *J. Neurosci.* **24**, 4070-4081.
Mashukova, A., Forteza, R., Wald, F. A. and Salas, P. J. (2012). PDK1 in apical signaling endosomes participates in the rescue of the polarity complex atypical PKC by intermediate filaments in intestinal epithelia. *Mol. Biol. Cell* **23**, 1664-1674.
Matsui, T., Maeda, M., Doi, Y., Yonemura, S., Amano, M., Kaibuchi, K., Tsukita, S. and Tsukita, S. (1998). Rho-kinase phosphorylates COOH-terminal threonines of ezrin/radixin/moesin (ERM) proteins and regulates their head-to-tail association. *J. Cell Biol.* **140**, 647-657.
McConnell, R. E., Higginbotham, J. N., Shifrin, D. A., Jr, Tabb, D. L., Coffey, R. J. and Tyska, M. J. (2009). The enterocyte microvillus is a vesicle-generating organelle. *J. Cell Biol.* **185**, 1285-1298.
Müller, T., Hess, M. W., Schiefermeier, N., Pfaller, K., Ebner, H. L., Heinz-Erian, P., Ponstingl, H., Partsch, J., Röllinghoff, B., Köhler, H. et al. (2008). MYO5B mutations cause microvillus inclusion disease and disrupt epithelial cell polarity. *Nat. Genet.* **40**, 1163-1165.
Phillips, A. D. and Schmitz, J. (1992). Familial microvillous atrophy: a clinicopathological survey of 23 cases. *J. Pediatr. Gastroenterol. Nutr.* **14**, 380-396.
Phillips, A. D., Jenkins, P., Raafat, F. and Walker-Smith, J. A. (1985). Congenital microvillous atrophy: specific diagnostic features. *Arch. Dis. Child.* **60**, 135-140.
Phillips, A. D., Brown, A., Hicks, S., Schüller, S., Murch, S. H., Walker-Smith, J. A. and Swallow, D. M. (2004). Acetylated sialic acid residues and blood group antigens localise within the epithelium in microvillous atrophy indicating internal accumulation of the glycocalyx. *Gut* **53**, 1764-1771.
Pollock, S., Antrobus, R., Newton, L., Kampa, B., Rossa, J., Latham, S., Nichita, N. B., Dwek, R. A. and Zitzmann, N. (2010). Uptake and trafficking of liposomes to the endoplasmic reticulum. *FASEB J.* **24**, 1866-1878.
Provance, D. W., Jr, Addison, E. J., Wood, P. R., Chen, D. Z., Silan, C. M. and Mercer, J. A. (2008). Myosin-Vb functions as a dynamic tether for peripheral endocytic compartments during transferrin trafficking. *BMC Cell Biol.* **9**, 44.
Roland, J. T., Bryant, D. M., Datta, A., Itzen, A., Mostov, K. E. and Goldenring, J. R. (2011). Rab GTPase-Myo5B complexes control membrane recycling and epithelial polarization. *Proc. Natl. Acad. Sci. USA* **108**, 2789-2794.
Ruemmele, F. M., Schmitz, J. and Goulet, O. (2006). Microvillous inclusion disease (microvillous atrophy). *Orphanet J. Rare Dis.* **1**, 22.
Sabherwal, N., Tsutsui, A., Hodge, S., Wei, J., Chalmers, A. D. and Papalopulu, N. (2009). The apicobasal polarity kinase aPKC functions as a nuclear determinant and regulates cell proliferation and fate during Xenopus primary neurogenesis. *Development* **136**, 2767-2777.
Saotome, I., Curto, M. and McClatchey, A. I. (2004). Ezrin is essential for epithelial organization and villus morphogenesis in the developing intestine. *Dev. Cell* **6**, 855-864.
Schuh, M. (2011). An actin-dependent mechanism for long-range vesicle transport. *Nat. Cell Biol.* **13**, 1431-1436.
Shifrin, D. A., Jr, McConnell, R. E., Nambiar, R., Higginbotham, J. N., Coffey, R. J. and Tyska, M. J. (2012). Enterocyte microvillus-derived vesicles detoxify bacterial products and regulate epithelial-microbial interactions. *Curr. Biol.* **22**, 627-631.
Shin, H.-W., Morinaga, N., Noda, M. and Nakayama, K. (2004). BIG2, a guanine nucleotide exchange factor for ADP-ribosylation factors: its localization to recycling endosomes and implication in the endosome integrity. *Mol. Biol. Cell* **15**, 5283-5294.
Shiue, H., Musch, M. W., Wang, Y., Chang, E. B. and Turner, J. R. (2005). Akt2 phosphorylates ezrin to trigger NHE3 translocation and activation. *J. Biol. Chem.* **280**, 1688-1695.
Szperl, A. M., Golachowska, M. R., Bruinenberg, M., Prekeris, R., Thunnissen, A.-M. W. H., Karrenbeld, A., Dijkstra, G., Hoekstra, D., Mercer, D., Ksiazyk, J. et al. (2011). Functional characterization of mutations in the myosin Vb gene associated with microvillus inclusion disease. *J. Pediatr. Gastroenterol. Nutr.* **52**, 307-313.
ten Klooster, J. P., Jansen, M., Yuan, J., Oorschot, V., Begthel, H., Di Giacomo, V., Colland, F., de Koning, J., Maurice, M. M., Hornbeck, P. et al. (2009). Mst4 and Ezrin induce brush borders downstream of the Lkb1/Strad/Mo25 polarization complex. *Dev. Cell* **16**, 551-562.
Viswanatha, R., Ohouo, P. Y., Smolka, M. B. and Bretscher, A. (2012). Local phosphocycling mediated by LOK/SLK restricts ezrin function to the apical aspect of epithelial cells. *J. Cell Biol.* **199**, 969-984.
Wakabayashi, Y., Dutt, P., Lippincott-Schwartz, J. and Arias, I. M. (2005). Rab11a and myosin Vb are required for bile canalicular formation in WIF-B9 cells. *Proc. Natl. Acad. Sci. USA* **102**, 15087-15092.
Wald, F. A., Oriolo, A. S., Mashukova, A., Fregien, N. L., Langshaw, A. H. and Salas, P. J. I. (2008). Atypical protein kinase C (iota) activates ezrin in the apical domain of intestinal epithelial cells. *J. Cell Sci.* **121**, 644-654.
Wang, W., Soroka, C. J., Mennone, A., Rahner, C., Harry, K., Pypaert, M. and Boyer, J. L. (2006). Radixin is required to maintain apical canalicular membrane structure and function in rat hepatocytes. *Gastroenterology* **131**, 878-884.
Winter, J. F., Höpfner, S., Korn, K., Farnung, B. O., Bradshaw, C. R., Marsico, G., Volkmer, M., Habermann, B. and Zerial, M. (2012). Caenorhabditis elegans screen reveals role of PAR-5 in RAB-11-recycling endosome positioning and apicobasal cell polarity. *Nat. Cell Biol.* **14**, 666-676.
Zhu, L., Hatakeyama, J., Chen, C., Shastri, A., Poon, K. and Forte, J. G. (2008). Comparative study of ezrin phosphorylation among different tissues: more is good; too much is bad. *Am. J. Physiol.* **295**, C192-C202.